Correlations and firing rates of pyramidal neuron dendrites

Robert Gowers
Mathematics for Real-World Systems CDT, University of Warwick
(Dated: September 19, 2016)

A dendrite was modelled in the subthreshold regime using the cable equation with both white and filtered synaptic input for passive and resonant membranes. Analytical expressions for the variance could be readily obtained in all four cases, and a theoretical approximation for the firing rate was found for filtered noise. Resonance was found to decrease the variance, but could increase or decrease the firing rate depending on the threshold level relative to the noise strength.

I. INTRODUCTION

Pyramidal neurons are a subject of active interest due to their prominence in the neocortex, which has an important role in cognition. Each pyramidal cell has on the order of 10^4 synapses [1], and it is thought that the integration of this synaptic information is what gives the neocortex its computational power [2].

Models for the variance and firing statistics of neurons usually treat the neuron as a point-like object with a single membrane potential. However, the typical length of a pyramidal neuron is comparatively large at about 1 mm, with each of the dendrites in excess of 100 µm [2]. This means that in order to describe their internal behaviour, a spatially dependent membrane potential is required.

Production of a spike due to the membrane potential exceeding a certain threshold can occur not only as an action potential at the soma of a neuron but also at excitable patches located in the dendrites, where they are known as dendritic spikes. Pyramidal neurons have been found to contain many such excitable patches [3]. Furthermore, since the opening of ion channels is inherently noisy, the exact strength and arrival time of synaptic impulses is a stochastic process [4], leading to fluctuations in the potential across the neuron. Therefore, it is important to know how the potential fluctuates along the length of the neuron in order to ascertain which locations the production of dendritic spikes is most likely.

Furthermore, in the subthreshold regime, pyramidal neurons have been found to attenuate synaptic inputs differently depending on their input frequency [5], acting like a bandpass filter. In particular, this behaviour is observed in the apical dendrites, with other dendrites being more passive [6]. This resonant behaviour is likely important for synaptic integration and the firing rate.

This report explores a spatially distributed, stochastic resonant membrane model applied to a single dendrite in the subthreshold regime with progressively increasing levels of complexity. First, a model with white synaptic noise is outlined for both a passive and a resonant membrane. Then, a filtered synaptic noise model is investigated for both membrane types. For each model, the variance of the potential is derived and verified by numerical simulation. The firing rate for white noise is simulated using a threshold-reset method, where if the potential at a defined trigger point reaches threshold, the potential is reset. While for filtered noise, the firing rate of the dendrite is approximated using the upcrossing method, which has previously been used for point neurons [7] but not for a dendrite.

While a spatially distributed white noise model with a passive membrane has already been investigated [8], models with resonant membranes and filtered synaptic noise have not been subject to the same theoretical treatment. Thus, this report aims to expand the theoretical understanding of single neuron behaviour by including resonance and filtered noise.

II. GENERAL CABLE EQUATION

The models explored will assume that the dendrite is a cylinder of constant radius a and finite length L. The membrane conductance per unit area g_L, the membrane capacitance per unit area c and the axial resistivity of the dendrite r_a are also assumed to be constant along the axial length of the dendrite X. By considering a short length of cable Δ_X, conservation of current gives the familiar cable equation for the membrane potential V [9],

$$\tau\frac{\partial V}{\partial T}+V-E_L-\lambda^2\frac{\partial^2 V}{\partial X^2}=\frac{\Delta I}{2\pi a\Delta_X g_L}, \qquad (1)$$

where E_L is the reversal potential, ΔI is the current injected into the membrane, $\tau = c/g_L$ is the voltage time constant and $\lambda^2 = a/(2r_a g_L)$ is the length constant.

The synaptic current, I_{syn}, forms part of ΔI and is due to the opening of ion channels in the membrane. These channels open and close stochastically, with the opening of a channel being represented by a change in the conductance to their ionic species. Denoting excitatory and inhibitory synapses by e and i respectively, with conductances $G_{e,i}$ and reversal potentials $E_{e,i}$, the synaptic current can be written as,

$$I_{\text{syn}} = G_e(E_e - V) + G_i(E_i - V). \qquad (2)$$

III. WHITE NOISE MODEL

For the white noise model, ion channels open and close instantaneously. This results in the conductances $G_{e,i}$

also changing instantaneously, so I_{syn} is considered proportional to the stochastic process which opens the ion channels. This means that I_{syn} can be represented by a series of randomly arriving pulses.

Due to the large number of synapses located on the membrane, a continuum limit of their distribution is chosen. Let ρ_s denote the density of synapses per unit area and r_s the rate at which pulses arrive. Assuming that pulses arrive independently and are identically distributed across the length of the dendrite, the number of pulses, Z_j, which arrive in a time Δ_T on an area $2\pi\Delta_X$ is Poisson distributed, with the mean N_s given by,

$$N_s = 2\pi a \Delta_X \rho_s r_s \Delta_T. \tag{3}$$

Letting $\{T_k\}$ be the set of pulse arrival times and q_s the charge delivered per active synapse, the incoming current is

$$\begin{aligned} I_{\text{syn}} &= q_s \sum_{\{T_k\}} \delta(T - T_k) \\ &= \frac{q_s}{\Delta_T} \int_T^{T+\Delta_T} dT' \sum_{\{T_k\}} \delta(T' - T_k) = \frac{q_s Z_j}{\Delta_T}. \end{aligned} \tag{4}$$

In the limit of a large number of pulses, Z_j can be approximated by a Gaussian distribution with mean and variance N_s. Letting ϕ denote a zero mean, unit variance Gaussian random number, this means that,

$$\begin{aligned} I_{\text{syn}} &\approx \frac{q_s}{\Delta_T}(N_s + \sqrt{N_s}\phi) \\ &= 2\pi a \Delta_X q_s \left(\rho_s r_s + \sqrt{\frac{\rho_s r_s}{2\pi a}} \frac{\phi}{\sqrt{\Delta_X \Delta_T}} \right). \end{aligned} \tag{5}$$

To obtain a stochastic differential equation, we define the white noise term as,

$$\xi(X,T) = \lim_{\Delta_X \to 0, \Delta_T \to 0} \frac{\phi}{\sqrt{\Delta_X \Delta_T}}, \tag{6}$$

which is zero mean, $\langle \xi \rangle = 0$, and delta-correlated in time and space, $\langle \xi(X,T)\xi(X',T') \rangle = \delta(X - X')\delta(T - T')$. Note that in this report $\langle . \rangle$ denotes an expectation over realisations of the process.

A. Passive Membrane

1. Cable Equation

A passive membrane can be modelled entirely by its membrane conductance and capacitance. Therefore, only the synaptic current needs to be considered, meaning that $\Delta I = \Delta I_{\text{syn}}$. Substituting (5) into (1) gives,

$$\begin{aligned} &\tau \frac{\partial V}{\partial T} = E - V + \lambda^2 \frac{\partial^2 V}{\partial X^2} + 2\sigma_\infty \sqrt{\lambda\tau}\,\xi(X,T), \\ &E = E_L + q_s \rho_s r_s / g_L, \quad \sigma_\infty = \frac{q_s}{2g_L} \sqrt{\frac{\rho_s r_s}{2\pi a \lambda \tau}}. \end{aligned} \tag{7}$$

Rescaling voltage with $v = (V - E)/\sigma_\infty$ and using dimensionless units for space and time ($X = \lambda x$, $T = \tau t$) yields,

$$\boxed{\frac{\partial v}{\partial t} = -v + \frac{\partial^2 v}{\partial x^2} + 2\xi(x,t).} \tag{8}$$

2. Variance

In the subthreshold regime it assumed there is enough time for the distribution of the potential to equilibrate. This means that the steady state variance $\langle v(x)^2 \rangle$ for a finite length of cable L with sealed ends is of particular interest. Here, sealed ends refers to enforcing the zero current boundary conditions, $\frac{\partial v}{\partial x}(x = 0) = 0 = \frac{\partial v}{\partial x}(x = l)$, where l is the scaled length of the cable with $L = \lambda l$. Sealed ends were chosen because it provides a simple boundary condition for an unconnected dendrite.

To calculate the variance, the voltage and white noise terms will be decomposed into different modes:

$$v(x,t) = \sum_{n=0}^{\infty} v_n(t)\phi_n(x), \quad \xi(x,t) = \sum_{n=0}^{\infty} \xi_n(t)\phi_n(x), \tag{9}$$

where $\xi_n(t) = \int_0^l \xi(x,t)\phi_n(x)dx$ and the eigenfunctions ϕ_n are chosen to be orthonormal to each other such that,

$$\int_0^l \phi_n(x)\phi_m(x)dx = \delta_{mn}, \tag{10}$$

where δ_{mn} in this case is the Kronecker delta function. For a cable with sealed ends the eigenfunctions are given by,

$$\phi_n(x) = \begin{cases} \frac{1}{\sqrt{l}} & n = 0 \\ \sqrt{\frac{2}{l}} \cos\left(\frac{n\pi x}{l}\right) & n = 1, 2, \ldots \end{cases}. \tag{11}$$

Substituting the components of v_n into (8) yields:

$$\frac{dv_n}{dt} = -\mu_n v_n + 2\xi_n(t), \quad \mu_n = 1 + \frac{n^2\pi^2}{l^2}. \tag{12}$$

From this one can immediately see that $\langle v_n \rangle = 0$ and hence $\langle v \rangle = 0$. The variance for v as a whole is given by

$$\begin{aligned} \langle v(x,t)v(y,t) \rangle &= \langle \sum_{n=0}^{\infty} \phi_n(x)v_n(t) \sum_{m=0}^{\infty} \phi_m(y)v_m(t) \rangle \\ &= \sum_{n=m} \langle v_n(t)^2 \rangle \phi_n(x)^2 \\ &\quad + \sum \sum_{n \neq m} \langle v_n(t)v_m(t) \rangle \phi_n(x)\phi_m(x) \\ &= \sum_{n=0}^{\infty} \langle v_n(t)^2 \rangle \phi_n(x)^2. \end{aligned} \tag{13}$$

Given that $\langle v \rangle = 0$, it is evident that in order to obtain the overall variance, one only needs to calculate an expression for the mode variance $\langle v_n^2 \rangle$. To obtain the variance of each mode, we first must note that $\langle \xi_n(t)\xi_m(t') \rangle = \delta(t-t')\delta_{mn}$, which can be easily derived from (9) and (10). The solution of (12) is given as,

$$v_n(t) = 2\int_0^t dt' e^{-\mu_n(t-t')}\xi_n(t'), \tag{14}$$

which gives the mode variance as,

$$\langle v_n(t)^2 \rangle = \frac{2}{\mu_n}(1 - e^{-2\mu_n t}). \tag{15}$$

Substituting for $\phi_n(x)$ and $\langle v_n(t)^2 \rangle$ in (13) while letting $t \to \infty$ to obtain the steady state yields,

$$\langle v(x)v(y) \rangle = \frac{2}{l}\left[1 + 2\sum_{n=1}^{\infty}\frac{1}{\mu_n}\cos^2\left(\frac{n\pi x}{l}\right)\right]. \tag{16}$$

The summation can be performed using the following results [10],

$$\sum_{n=1}^{\infty}\frac{1}{\beta^2+n^2} = \frac{\pi}{2\beta}\coth(\pi\beta) - \frac{1}{2\beta^2}$$
$$\sum_{n=1}^{\infty}\frac{\cos(nz)}{\beta^2+n^2} = \frac{\pi}{2\beta}\frac{\cosh[\beta(\pi-z)]}{\sinh(\beta\pi)} - \frac{1}{2\beta^2}, \tag{17}$$

which gives the variance as:

$$\boxed{\langle v(x)^2 \rangle = \frac{2\cosh(l-x)\cosh x}{\sinh l}.} \tag{18}$$

This is the same result as that derived by Tuckwell via Green's functions [8]. This represents a hyperbolic variance in space which has a minimum at $x = l/2$ and is greatest at the ends.

Numerical simulations were performed to verify the derived expression for the variance. All plots of simulations will use the convention of points representing simulated values while solid lines represent the corresponding theoretical result. To see the effect of changing the cable length, it is computationally more convenient to use the unscaled length L and varying λ to achieve this effect. Therefore, in all future simulations a biophysically reasonable length of dendrite of 100 µm is considered [11].

Simulations were performed using the forward Euler-Maruyama method to approximate the cable equation. Through this method, $\phi/\sqrt{\Delta_X \Delta_t}$ was used to approximate $\xi(X,t)$ for chosen space and time steps Δ_X and Δ_t. A forward difference method was used to approximate all the temporal derivatives, while a second order central difference scheme was used for the spatial derivative. Since the system is ergodic once it reaches the steady state, a single realisation of each process was used, meaning that variances could be calculated over time rather than realisations.

For the passive cable with white noise, the aim was to see how the variance changed with different λ. In this case biophysically reasonable values of $\lambda = 10\,\mu\text{m}, 20\,\mu\text{m}$ and $50\,\mu\text{m}$ [11] were used. FIG. 1a shows that as λ increases, the diffusive effect is greater and the variance increases. As $\lambda \to 0$, $\langle v(x)^2 \rangle \to 1$ for $x \neq 0, L$ and $\langle v(0)^2 \rangle \to 2$, $\langle v(L)^2 \rangle \to 2$. On the other hand, as $\lambda \to \infty$, $\langle v(x)^2 \rangle$ increases without bound.

3. Firing Rate Simulation

The firing rate of a cable subject to white noise was simulated using a threshold-reset method with a single trigger point x_0. This was achieved by numerically simulating the evolution of the potential as before, but whenever $v(x_0)$ exceeds the threshold v_{th}, the potential across the whole dendrite is reset to zero. The firing rate is then obtained by dividing the number of times the cable is reset by the total time. To find how the firing rate depends on x_0, this process is repeated with a different value of x_0 each time.

As with the variance simulations, the effect of changing λ on the firing rate was observed, with a constant threshold $v_{\text{th}} = 1$. Note that unlike the variance, there is no easily obtainable theoretical result for comparison. Although approaches using the first passage time can be used as an approximation to the firing rate, these are usually computationally inefficient since they involve numerically solving PDEs with at least 3 dimensions [8].

FIG. 1b shows that as λ is increased, the firing rate also increases. Intuitively this makes sense as the variance increases with λ and one would expect a greater firing rate with stronger fluctuations. However, while the rate is greatest at the ends, a small maximum at $X = 50\,\mu\text{m}$ is consistently observed where the variance is at a minimum. This indicates that the firing rate does not simply monotonically increase with the variance.

B. Resonant Membrane

1. Cable Equation

A resonant membrane has an inductive circuit branch which arises from voltage dependent ionic conductances [12]. This inductive branch is described by an inductance L_h in series with a resistance R_h, as shown in FIG. 2. The active current I_h through this branch is described by,

$$L_h\frac{dI_h}{dT} = V - E_L - R_h I_h. \tag{19}$$

In principle, one can consider multiple inductive branches corresponding to various different types of ionic species relevant to the membrane. For simplicity, we will use just one inductive branch.

For the resonant cable, $\Delta I = I_{\text{syn}} - I_h$. In order to extend the equivalent circuit across to a whole cable, it

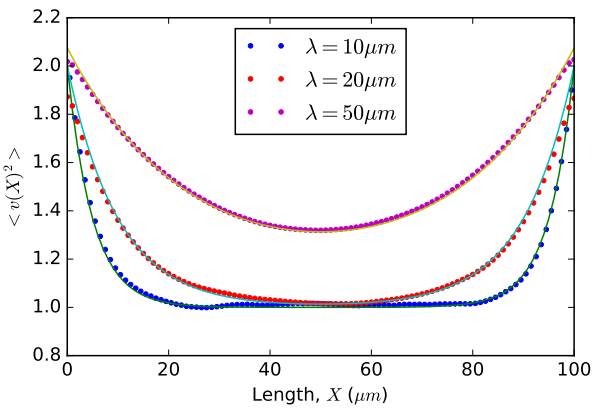

(a) Variance.

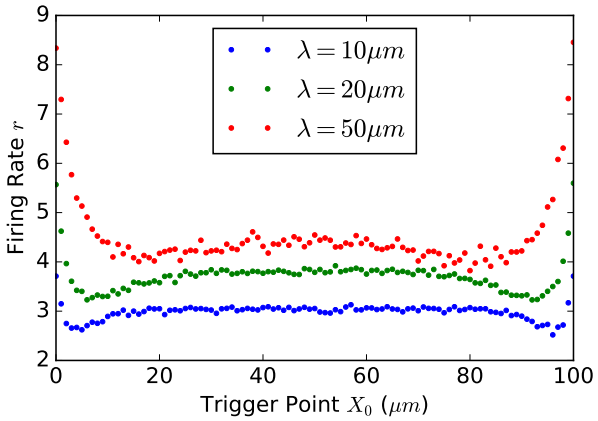

(b) Firing rate for $v_{th} = 1.0$.

FIG. 1: Variance and firing rate for a passive cable subject to white noise.

is more convenient to consider it in terms of the conductance $G_h = R_h^{-1}$ and the inverse inductance $P_h = L_h^{-1}$. Denoting the conductance per unit area as g_h, the inverse inductance per unit area as p_h and the active current density as W, we can rewrite our bulk quantities in terms of densities as follows:

$$I_h = 2\pi a \Delta_X W, \;\; G_h = 2\pi a \Delta_X g_h, \;\; P_h = 2\pi a \Delta_X p_h. \tag{20}$$

Provided that g_h and p_h remain constant throughout the cable, we can use (20) in the cable equation (1) along with (5), to obtain,

$$\boxed{\begin{aligned} \frac{\partial v}{\partial t} &= \frac{\partial^2 v}{\partial x^2} - v - \kappa w + 2\xi(x,t) \\ \alpha_w \frac{\partial w}{\partial t} &= v - w. \end{aligned}} \tag{21}$$

However, in this case the variables are scaled differently to (8):

$$\begin{aligned} v &= \frac{V - \tilde{E}_v}{\sigma_\infty}, \quad \tilde{E}_v = E_L + \frac{E_s g_L}{g_h + g_L}, \quad E_s = q_s \rho_s r_s / g_L, \\ w &= \frac{W - \tilde{E}_w}{g_h \sigma_\infty}, \quad \tilde{E}_w = \frac{E_s g_h g_L}{g_h + g_L}, \end{aligned} \tag{22}$$

with σ_∞ defined as before. Hereafter w will be referred to as the active variable. $\alpha_w = g_h/(\tau p_h)$ is the effective ratio of the active variable time constant to the potential time constant, with $\alpha_w > 1$ meaning that w reacts more slowly than v. $\kappa = g_h/g_L$ acts as the coupling parameter between the active current and the membrane potential. x and t are defined as before.

Note that when $\kappa = 0$, the equations in (21) are uncoupled and we obtain (8). Also when $\alpha_w \to \infty$, the active variable acts too slowly to affect the potential and the passive equation is again obtained.

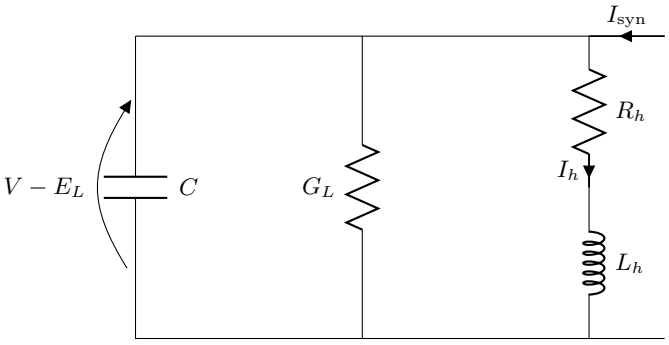

FIG. 2: Resonant membrane equivalent circuit.

2. *Variance*

For the resonant cable, the active variable is also split into modes, giving the decomposed cable equation as,

$$\begin{aligned} \frac{dv_n}{dt} &= -\mu_n v_n - \kappa w_n \\ \alpha_w \frac{dw_n}{dt} &= v_n - w_n. \end{aligned} \tag{23}$$

Taking temporal Laplace transforms of (23) yields,

$$\tilde{v}_n(\omega) = \frac{2(1 + \alpha_w \omega)\tilde{\xi}_n(\omega)}{(\omega + \mu_n)(1 + \alpha_w \omega) + \kappa} = 2\tilde{A}_n(\omega)\tilde{\xi}_n(\omega). \tag{24}$$

To invert $\tilde{A}_n(\omega)$ for use in the convolution theorem, we will rearrange it to give,

$$\begin{aligned} \tilde{A}_n(\omega) &= \frac{\omega + a}{(\omega + a)^2 + \Omega^2} + \frac{b\Omega}{(\omega + a)^2 + \Omega^2}, \\ a = \frac{1 + \alpha_w \mu_n}{2\alpha_w}, \quad \Omega &= \frac{\mu_n + \kappa}{\alpha_w} - a^2, \quad b = \frac{1/\alpha_w - a}{\Omega}. \end{aligned} \tag{25}$$

The steady state mode variance is therefore:

$$\langle v_n^2 \rangle = 4 \int_0^\infty A_n(t')^2 dt' = 2 \frac{1 + \alpha_w(\mu_n + \kappa)}{(1 + \alpha_w \mu_n)(\mu_n + \kappa)}. \tag{26}$$

Using (13) and (17), we can obtain the whole steady state variance as:

$$\boxed{\langle v(x)^2\rangle = \frac{C(x;\kappa) - \alpha_w \kappa C(x;1/\alpha_w)}{1-\alpha_w\kappa},} \tag{27}$$

where $C(x;\zeta)$ is defined as,

$$C(x;\zeta) = \frac{2\cosh((l-x)\sqrt{1+\zeta})\cosh(x\sqrt{1+\zeta})}{\sqrt{1+\zeta}\sinh(l\sqrt{1+\zeta})}. \tag{28}$$

(27) reduces to the variance for the passive cable for $\kappa = 0$ or $\alpha_w = \infty$, as would be expected. Note that resonance decreases the variance of the potential and the effective length constant, equivalent to decreasing λ.

In simulations of a resonant cable with white noise, the effect of changing α_w was observed with values of $\alpha_w = 0.1$, 1 and 10. A biophysically reasonable value for a resonant neuron of $\kappa = 0.85$ [13] was used for each simulation, as was $\lambda = 20\,\mu\text{m}$. As shown in FIG. 3a and predicted earlier, as α_w increases, the variance also increases.

3. Firing Rate Simulation

The firing rate was simulated for the resonant membrane in the same manner as the passive membrane. This time λ and v_{th} were kept constant at 20 µm and 1 respectively, while α_w was varied in the same way as for the variance.

FIG. 3b shows that, like the passive membrane, the firing rate is highest for a trigger point at the ends and has a maximum at the centre. However, while one might expect that decreasing α_w, which decreases $\langle v(x)^2\rangle$, would reduce the firing rate, the opposite effect is seen. This again implies that the white noise firing rate at x_0 is more complex than simply increasing with the variance at x_0.

IV. FILTERED NOISE MODEL

For filtered synaptic noise, the channels do not open instantaneously. This in turn means that the synaptic conductance does not change instantaneously and hence the rate at which the synaptic conductance changes is proportional to the stochastic process. This has the effect of smoothing the way in which the potential fluctuates.

Each synapse becomes activated at a rate r_s $(s = e, i)$ with ρ_s again being the density of synapses per unit area. Thus the mean number of incoming pulses over a small area of dendrite $2\pi\Delta_X$ and in a time Δ_T, N_s, is given by (3) as in the white synaptic noise case. The difference now is that each pulse causes a step increase in the synaptic conductance of γ_s and that such changes are assumed to decay exponentially with time constant τ_s, in the same way as [14], giving:

$$\tau_s \frac{\partial G_s}{\partial T} = -G_s + \tau_s\gamma_s \sum_{\{T_{sk}\}} \delta(T - T_{sk}). \tag{29}$$

Here we use the Gaussian approximation for a large number of pulses as seen for white synaptic noise in equation (5),

$$\tau_s \frac{\partial G_s}{\partial T} \approx -G_s + \frac{\tau_s\gamma_s}{\Delta_T}(N_s + \sqrt{N_s}\phi)$$
$$= -G_s + 2\pi a \Delta_X \tau_s \gamma_s \left(\rho_s r_s + \sqrt{\frac{\rho_s r_s}{2\pi a}}\frac{\phi}{\sqrt{\Delta_X\Delta_T}}\right). \tag{30}$$

A. Passive Membrane

1. Cable Equation

Writing $G_s = 2\pi a \Delta_X g_s$, substitution of (30) into the general cable equation with $\Delta I = I_{\text{syn}}$ gives,

$$c\frac{\partial V}{\partial T} = g_L(E_L - V) + g_e(E_e - V) + g_i(E_i - V) + g_L\lambda^2\frac{\partial^2 V}{\partial X^2}$$
$$\tau_s\frac{\partial g_s}{\partial T} = -g_s + \tau_s\gamma_s\left(\rho_s r_s + \sqrt{\frac{\rho_s r_s}{2\pi a}}\xi_s(X,T)\right), \tag{31}$$

using the definition of $\xi_s(X,T)$ as before, the subscript implying that ξ_i and ξ_e are distinct stochastic processes. We now separate the potential and conductances into deterministic, $(\overline{V}, \overline{g_s})$, and stochastic, $(v,\ g_{sF})$, components with $V = \overline{V} + v$ and $g_s = \overline{g_s} + g_{sF}$. Defining $g_0 = g_L + \overline{g_e} + \overline{g_i}$, $E_0 = (g_L E_L + \overline{g_e}E_e + \overline{g_i}E_i)/g_0$, $g_0\lambda_0^2 = g_L\lambda^2$ and $\tau_0 = c/g_0$, for the deterministic part we obtain:

$$\tau_0\frac{\partial\overline{V}}{\partial T} = E_0 - \overline{V} + \lambda_0^2\frac{\partial^2 V}{\partial X^2}$$
$$\tau_s\frac{\partial\overline{g_s}}{\partial T} = -\overline{g_s} + \tau_s\gamma_s\rho_s r_s. \tag{32}$$

To write the equations for the stochastic components, we first make the assumption that the fluctuations in the conductance are small in comparison to the deterministic value, meaning that $g_{sF}\times v$ terms are small and can be neglected. This assumption leads to,

$$\tau_0\frac{\partial v}{\partial T} = -v + \frac{g_{eF}}{g_0}(E_e - \overline{V}) + \frac{g_{iF}}{g_0}(E_i - \overline{V}) + \lambda_0^2\frac{\partial^2 v}{\partial X^2}$$
$$\tau_s\frac{\partial g_{sF}}{\partial T} = -g_{sF} + \tau_s\gamma_s\sqrt{\frac{\rho_s r_s}{2\pi a}}\xi_s(X,T). \tag{33}$$

Of particular interest is the spatially uniform steady state, where, for the deterministic components $\overline{V} = E_0$ and $\overline{g_s} = \tau_s\gamma_s\rho_s r_s$ across the whole length of the cable. Note that this also makes τ_0 and g_0 constants rather than varying in time. Defining,

$$u_s = \frac{g_{sF}(E_s - E_0)}{g_0}, \quad 2\sigma_s = \frac{\tau_s\gamma_s(E_s - E_0)}{g_0}\sqrt{\frac{\rho_s r_s}{2\pi a\lambda_0\tau_0}},$$
$$x = X/\lambda_0, \quad t = T/\tau_0, \quad \alpha_s = \tau_s/\tau_0, \tag{34}$$

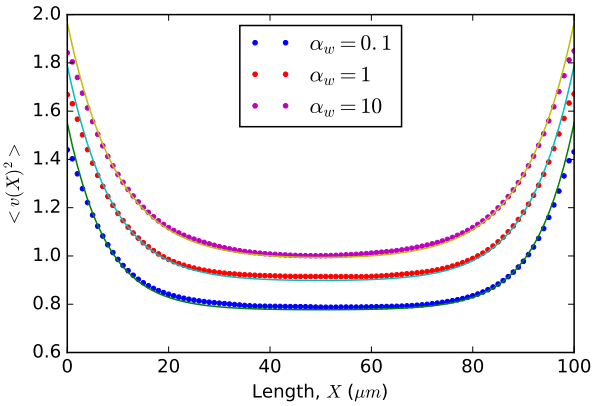

(a) Variance for $\lambda = 20\,\mu\text{m}$,$\kappa = 0.85$.

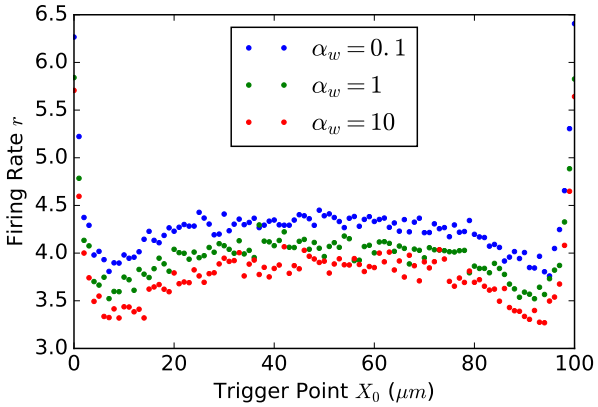

(b) Firing rate for $\lambda = 20\,\mu\text{m}$, $v_{th} = 1.0$.

FIG. 3: Variance and firing rate for a resonant cable subject to white noise.

yields the final set of equations for the passive filtered cable:

$$\boxed{\begin{aligned} \frac{\partial v}{\partial t} &= -v + u_e + u_i + \frac{\partial^2 v}{\partial x^2} \\ \alpha_e \frac{\partial u_e}{\partial t} &= -u_e + 2\sigma_e \xi_e(x,t) \\ \alpha_i \frac{\partial u_i}{\partial t} &= -u_i + 2\sigma_i \xi_i(x,t). \end{aligned}} \tag{35}$$

Hereafter $u_{e,i}$ will be referred to as conductance variables. Note when considering one conductance variable, taking $\alpha_s \to 0$, we obtain the white noise limit, since the conductance responds instantaneously to fluctuations. On the other hand, for $\alpha_s \to \infty$, stochastic effects are decoupled from the potential and the cable equation is deterministic.

2. *Variance*

For the passive cable with filtered noise, the conductance variables will be split the into modes in the same manner as white noise. Hence in addition to (9), we also have

$$u_e(x,t) = \sum_{n=0}^{\infty} \phi_n(x) u_{en}(t), \quad u_i(x,t) = \sum_{n=0}^{\infty} \phi_n(x) u_{in}(t). \tag{36}$$

As with white noise (13) applies, so it is sufficient to find the variance of each mode to find the variance of v. Decomposing (35) into modes gives:

$$\frac{dv_n}{dt} = -\mu_n v_n + u_{en} + u_{in}, \quad \alpha_s \frac{du_{sn}}{dt} = -u_{sn} + 2\sigma_e \xi_{sn}(t), \tag{37}$$

where μ_n is defined as before in (12). To combine the equations of (37) we will utilise the temporal Laplace transform, defined as,

$$\tilde{f}(\omega) = \int_0^{\infty} f(t) e^{-\omega t} dt. \tag{38}$$

Using this definition, taking temporal Laplace transforms of (37) gives,

$$\begin{aligned} \alpha_s \omega \tilde{u}_{sn} &= -\tilde{u}_{sn} + 2\sigma_s \tilde{\xi}_{sn}(\omega) \\ \tilde{v}_n(\omega)(\mu_n + \omega) &= \frac{2\sigma_e \tilde{\xi}_{en}(\omega)}{1 + \alpha_e \omega} + \frac{2\sigma_i \tilde{\xi}_{in}(\omega)}{1 + \alpha_i \omega}. \end{aligned} \tag{39}$$

Note that zero initial conditions have been assumed for all variables. Since the steady state is of interest, this is simply a matter of convenience. From (39), the convolution theorem can be used to extract $v_n(t)$,

$$v_{sn}(t) = 2\sigma_s \int_0^t A_{sn}(t - t') \xi_{sn}(t') dt', \tag{40}$$

where $v_n = v_{en} + v_{in}$ and $\tilde{A}_{sn}(\omega) = 1/[(\mu_n + \omega)(1 + \alpha_s \omega)]$. Here we will make the assumption that excitatory and inhibitory inputs are uncorrelated such that $\langle \xi_{en} \xi_{in} \rangle = 0$ for all time. However, it is possible to add a correlation coefficient between the two as can be seen in other studies [7].

Since we are looking at the steady state, we take $t \to \infty$ and obtain the mode variance as:

$$\langle v_n^2 \rangle = \langle v_{en}^2 \rangle + \langle v_{in}^2 \rangle = \frac{2\sigma_e^2}{\mu_n(1 + \alpha_e \mu_n)} + \frac{2\sigma_i^2}{\mu_n(1 + \alpha_i \mu_n)}. \tag{41}$$

Taking just one synaptic input type into consideration and summing as before, the variance can be found as,

$$\boxed{\langle v_s(x)^2 \rangle = \sigma_s^2 (C(x;0) - C(x;1/\alpha_s)).} \tag{42}$$

From this we can see that for $\sigma_s = 1$, the variance for filtered noise is lower than that of white noise. As $\alpha_s \to 0$, $C(x; 1/\alpha_s) \to 0$ and the filtered noise variance converges

to the white noise variance. Furthermore, as $\alpha_s \to \infty$, $\langle v_s(x)^2\rangle \to 0$, which would be expected from noise being decoupled from the system.

To see the effect of the filtered noise parameter α_s, λ was kept constant at 20 µm and α_s was given the values of 0.1, 1.1 and 2.2. $\sigma_s = 1$ was used for all simulations of the filtered noise model. Only one type of synaptic input was chosen, both for simplicity and to better compare with the white noise cases (for example $\sigma_e = 1$, $\sigma_i = 0.$). FIG. 4a confirms that as α_s becomes small, the variance increases towards the white noise limit.

3. Firing Rate Approximation

Provided that the time between firing events at a trigger point x_0 is sufficiently long, the firing rate can be approximated by the rate at which $v(x_0, t)$ crosses $v_{\rm th}$ with $\frac{\partial v}{\partial t} > 0$. This upcrossing method is desirable because it means that it is not necessary to consider the complex behaviour of a dendritic spike or to add a threshold and reset to the model.

The expected number of times the potential at a given location, $v(x_0, t')$, will cross $v_{\rm th}$ in a time interval $(0, t)$ is given by Rice's formula [15]:

$$n(t) = \int_0^t dt' \int_0^\infty \dot{v} p(v_{th}, \dot{v}; t') d\dot{v}, \tag{43}$$

where $\dot{v} = \frac{\partial v}{\partial t}$ and $p(v_{\rm th}, \dot{v}; t')$ is the joint probability density function of v and $\dot{v}$ evaluated at time t'. Note that in this case there is no reset after $v > v_{\rm th}$. In the steady state, the rate at which $v(x_0, t)$ crosses $v_{\rm th}$ is given by,

$$r = \int_0^\infty \dot{v} p(v_{\rm th}, \dot{v}) d\dot{v}. \tag{44}$$

For both the passive and resonant cables, it is evident that $\langle v\rangle = 0$ and $\langle \dot{v}\rangle = 0$. Furthermore in the steady state,

$$\langle v\frac{dv}{dt}\rangle = \langle \frac{1}{2}\frac{dv^2}{dt}\rangle = 0, \tag{45}$$

which implies that $\mathrm{cov}(v, \dot{v}) = 0$ and hence v and $\dot{v}$ are uncorrelated. Since both v and $\dot{v}$ are normally distributed (being based off Gaussian noise), this also means that they are independent of each other, meaning that $p(v_{\rm th}, \dot{v}) = p(v_{\rm th})p(\dot{v})$. This gives the firing rate approximation as:

$$\boxed{r(x_0) = \sqrt{\frac{\langle \dot{v}^2(x_0)\rangle}{\langle v^2(x_0)\rangle}} \frac{e^{-v_{\rm th}^2/2\langle v^2(x_0)\rangle}}{2\pi}.} \tag{46}$$

Thus to approximate the firing rate of the cable at a trigger point x_0, the variance of v and the variance of $\dot{v}$ need to be found.

Due to the upcrossing method requiring the variance of $\dot{v}$, it is not applicable to the white noise models. It can be shown that the evolution of v with time is not smooth and that, if one tries to numerically compute $\langle \dot{v}^2\rangle$, then this increases as the time step decreases. Therefore one can only apply the upcrossing method to models with filtered synaptic noise.

Since $\langle v^2\rangle$ has already been calculated, all that remains is to calculate $\langle \dot{v}^2\rangle$. Starting from the Laplace transform (39), one can see that,

$$\tilde{\dot{v}}_{sn}(\omega) = \frac{2\sigma_s \omega \tilde{\xi}_{sn}(\omega)}{(1+\alpha_s\omega)(\mu_n + \omega)} = 2\sigma_s \tilde{\xi}_{sn}(\omega)\tilde{A}_{sn}(\omega). \tag{47}$$

To obtain $\langle \dot{v}^2\rangle$, we can sum the mode variances in exactly the same way as for $\langle v^2\rangle$, since $\dot{v}$ satisfies the same spatial boundary conditions. This means that,

$$\begin{aligned}\langle \dot{v}_s(x)^2\rangle &= \sum_{n=0}^\infty \langle \dot{v}_{sn}^2\rangle \phi(x)^2 \\ &= \frac{2\sigma_s^2}{\alpha_s l}\left[\frac{1}{1+\alpha_s} + 2\sum_{n=1}^\infty \frac{1}{1+\alpha_s\mu_n}\cos^2\left(\frac{n\pi x}{l}\right)\right].\end{aligned} \tag{48}$$

This type of summation has been computed before for the resonant cable, and thus the variance of the time derivative is,

$$\langle \dot{v}_s(x)^2\rangle = \frac{\sigma_s^2}{\alpha_s^2} C(x; 1/\alpha_s), \tag{49}$$

with C defined as before. This means that the upcrossing rate of the passive filtered cable is:

$$\boxed{\begin{aligned} r(x_0) = \frac{1}{2\pi\alpha_s}\sqrt{\frac{C(x_0; 1/\alpha_s)}{C(x_0;, 0) - C(x_0; 1/\alpha_s)}} \\ \times \exp\left[\frac{-v_{\rm th}^2}{2\sigma_s^2[C(x_0;0) - C(x_0; 1/\alpha_s)]}\right].\end{aligned}} \tag{50}$$

This upcrossing method has been used before for point neurons with filtered noise [7] and for resonant point neurons [16] but not as yet for spatially distributed neurons. As discussed by Badel [7], the upcrossing method works best at approximating the firing rate for $\alpha_s \approx 1$ and also if $v_{\rm th}^2/\langle v^2(x_0)\rangle$ is not significantly smaller than 1. This is because small α_s causes the trajectory of $v(x_0, t)$ to become less smooth, causing there to be multiple upcrossing events in short succession where there would only be one firing event. On the other hand, for large α_s, the trajectory may stay above $v_{\rm th}$ for too long after crossing above it. Finally, if $v_{\rm th}^2/\langle v^2(x_0)\rangle$ is too small, then many of the firing events are also missed due to the trajectory staying above $v_{\rm th}$ for too long.

Simulations verifying the upcrossing rate were performed in a similar manner as the threshold-reset simulations, with the number of upcrossing events counted but without the potential being reset. For the passive membrane, α_s was kept at 1.1, while $v_{\rm th}$ was varied, with the

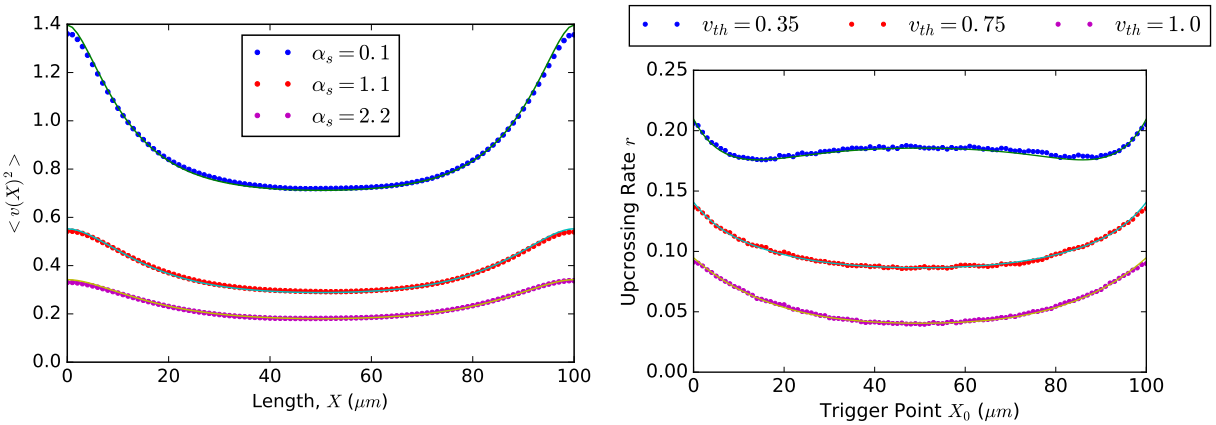

(a) Variance for $\lambda = 20\,\mu\text{m}$.

(b) Upcrossing rate for $\lambda = 20\,\mu\text{m}$, $\alpha_s = 1.1$.

FIG. 4: Variance and upcrossing rate for a passive cable subject to filtered noise.

values 0.35, 0.75 and 1. While $\sigma_s = 1$ was used, note that for $\alpha_s = 1.1$, $\langle v(x)^2 \rangle \sim 0.5$. Predictably, FIG. 4b shows that the upcrossing rate is higher when v_{th} is lower. However, it also shows that when v_{th} is sufficiently low, $r(x_0)$ has more turning points, as can be seen for $v_{\text{th}} = 0.35$, where there is a small maximum at $X = 50\,\mu\text{m}$. This is similar to the maximum observed for the white noise firing rate.

B. Resonant Membrane

1. Cable Equation

As in the unfiltered case, $\Delta I = I_{\text{syn}} - I_h$. With I_{syn}, W, g_h and p_h defined as before, substituting for ΔI gives the following system of equations:

$$\begin{aligned} c\frac{\partial V}{\partial T} &= g_L(E_L - V) + g_i(E_i - V) + g_e(E_e - V) \\ &\quad - W + g_L\lambda^2\frac{\partial^2 V}{\partial X^2} \\ \frac{1}{p_h}\frac{\partial W}{\partial T} &= -\frac{W}{g_h} + V - E_L \\ \tau_s\frac{\partial g_s}{\partial T} &= -g_s + \tau_s\gamma_s\left(\rho_s r_s + \sqrt{\frac{\rho_s r_s}{2\pi a}}\xi_s(X,T)\right). \end{aligned} \tag{51}$$

Now we separate the variables into deterministic and stochastic components in the same way as the passive membrane, with the addition of $W = \overline{W} + W_F$. The equations for the deterministic components are:

$$\begin{aligned} \tau_0\frac{\partial \overline{V}}{\partial T} &= E_0 - \overline{V} - \frac{\overline{W}}{g_0} + \lambda_0^2\frac{\partial^2 V}{\partial X^2} \\ \frac{1}{p_h}\frac{\partial \overline{W}}{\partial T} &= -\frac{\overline{W}}{g_h} + \overline{V} - E_L \\ \tau_s\frac{\partial \overline{g_s}}{\partial T} &= -\overline{g_s} + \tau_s\gamma_s\rho_s r_s, \end{aligned} \tag{52}$$

where g_0, E_0, τ_0 and λ_0 are defined the same as for the passive cable. For the stochastic components we again use the approximation that fluctuations in the conductance are small. In the spatially uniform steady state we have, $\overline{W} = g_h(\overline{V} - E_L)$, $\overline{V} = (E_0 g_0 + E_L g_h)/(g_0 + g_h)$ and $\overline{g_s} = \tau_s\gamma_s\rho_s r_s$. This means that the equations for the fluctuating components are,

$$\boxed{\begin{aligned} \frac{\partial v}{\partial t} &= -v + u_e + u_i - \kappa w + \frac{\partial^2 v}{\partial x^2} \\ \alpha_w\frac{\partial w}{\partial t} &= v - w \\ \alpha_s\frac{\partial u_s}{\partial t} &= -u_s + 2\sigma_s\xi_s(x,t), \end{aligned}} \tag{53}$$

where, x, t, α_s and σ_s are defined as before but now

$$\begin{aligned} u_s &= \frac{g_{sF}}{g_0}\left(E_s - \frac{E_0 g_0 + E_L g_h}{g_0 + g_h}\right), \quad w = \frac{W}{g_h}, \\ \alpha_w &= \frac{g_h}{\tau_0 p_h}, \quad \kappa = \frac{g_h}{g_0}. \end{aligned} \tag{54}$$

2. Variance

The derivation for the resonant filtered cable begins in the same way as the passive filtered cable; the variables in (53) are split into modes and Laplace transforms are taken:

$$\tilde{v}_n(\omega)\left[\mu_n + \omega + \frac{\kappa}{1 + \alpha_w\omega}\right] = \frac{2\sigma_e\tilde{\xi}_{en}(\omega)}{1 + \alpha_e\omega} + \frac{2\sigma_i\tilde{\xi}_{in}(\omega)}{1 + \alpha_i\omega}. \tag{55}$$

Dealing with one just type of synaptic input, we utilise the convolution theorem,

$$
\begin{aligned}
v_{sn}(t) &= 2\sigma_s \int_0^t A_{sn}(t-t')\xi_{sn}(t')dt', \\
\tilde{A}_{sn}(\omega) &= \frac{c_{1n}\omega + c_{2n}}{\kappa + (1+\alpha_w\omega)(\mu_n+\omega)} + \frac{c_{3n}}{1+\alpha_s\omega} \\
c_{1n} &= \frac{\alpha_w(\alpha_w-\alpha_s)}{\alpha_w + \alpha_s^2(\kappa+\mu_n) - \alpha_s(1+\alpha_w\mu_n)} \\
c_{2n} &= 1 + \frac{\alpha_s}{\alpha_w}(\kappa+\mu_n)c_{1n}, \quad c_{3n} = -\frac{\alpha_s}{\alpha_w}c_{1n}.
\end{aligned} \tag{56}
$$

In a similar fashion to the resonant unfiltered cable, the first term of $\tilde{A}_{sn}(\omega)$ can be split into two for an easier inverse transform:

$$
\begin{aligned}
\tilde{A}_{sn}(\omega) &= \frac{b_1(\omega+a)}{(\omega+a)^2+\Omega^2} + \frac{b_2\Omega}{(\omega+a)^2+\Omega^2} + \frac{b_3}{1/\alpha_s+\omega} \\
a &= \frac{1+\alpha_w\mu_n}{2\alpha_w}, \quad \Omega^2 = \frac{\mu_n+\kappa}{\alpha_w} - a^2, \quad b_1 = \frac{c_{1n}}{\alpha_w}, \\
b_2 &= \frac{c_{2n} - ac_{1n}}{\Omega\alpha_w}, \quad b_3 = \frac{c_{3n}}{\alpha_s},
\end{aligned} \tag{57}
$$

which means that the mode variance is given by

$$
\begin{aligned}
\langle v_{sn}^2 \rangle = \sigma_s^2 [&\frac{b_1^2(a^2+\Omega^2) + (ab_1+b_2\Omega)^2}{a(a^2+\Omega^2)} \\
&+ \frac{8b_3[b_1(a+1/\alpha_s)+b_2\Omega]}{(a+1/\alpha_s)^2+\Omega^2} + 2b_3^2\alpha_s].
\end{aligned} \tag{58}
$$

This yields the expression for the total variance as:

$$
\boxed{\langle v_s(x)^2 \rangle = \frac{2\sigma_s^2}{l}\left[h_0(\boldsymbol{c_0}) + 2\sum_{n=1}^{\infty} h_n(\boldsymbol{c_n}) \cos^2\left(\frac{n\pi x}{l}\right)\right],} \tag{59}
$$

where $\boldsymbol{c_n} = (c_{1n}, c_{2n}, c_{3n})$ and $h_n(\boldsymbol{c_n})$ is defined as:

$$
\begin{aligned}
h_n(\boldsymbol{c_n}) &= \frac{c_{1n}^2(\mu_n+\kappa) + c_{2n}^2\alpha_w}{\alpha_w(1+\alpha_w\mu_n)(\mu_n+\kappa)} \\
&+ \frac{4c_{3n}(c_{1n}+c_{2n}\alpha_s)}{\alpha_w + \alpha_s(1+\alpha_w\mu_n) + \alpha_s^2(\mu_n+\kappa)} + \frac{c_{3n}^2}{\alpha_s}.
\end{aligned} \tag{60}
$$

For the resonant membrane with filtered noise, simulations used values of $\alpha_s = 0.85$ $\kappa = 1.1$, while α_w was varied with the same values as for white noise. Again $\lambda = 20\,\mu\text{m}$ was chosen. As with white noise, FIG. 5a shows that α_w leads to a higher variance, meaning that resonance also lowers the variance for filtered noise. Furthermore note, that in comparison with FIG. 4a, while a greater conductance time constant lowers the variance, a greater active time constant has the opposite effect.

3. *Firing Rate Approximation*

With the resonant cable, the variance for $\dot{v}$ is also computed in a highly similar way to $\langle v^2 \rangle$,

$$
\begin{aligned}
\tilde{\dot{v}}_{sn}(\omega) &= \frac{2\sigma_s(1+\alpha_w\omega)\omega\tilde{\xi}_s(\omega)}{(1+\alpha_s\omega)[\kappa + (\mu_n+\omega)(1+\alpha_w\omega)]} \\
&= 2\sigma_s\tilde{\xi}_{sn}(\omega)\tilde{A}_{sn}(\omega) \\
\tilde{A}_{sn}(\omega) &= \frac{d_{1n}\omega + d_{2n}}{\kappa + (\mu_n+\omega)(1+\alpha_w\omega)} + \frac{d_{3n}}{1+\alpha_s\omega} \\
\alpha_s d_{1n} + \alpha_w d_{3n} &= \alpha_w, \quad d_{2n} = -(\mu_n+\kappa)d_{3n} \\
d_{3n} &= \frac{\alpha_w - \alpha_s}{\alpha_w - \alpha_s(1+\alpha_w\mu_n) + \alpha_s^2(\kappa+\mu_n)}.
\end{aligned} \tag{61}
$$

Therefore, in the same fashion as (58), the mode variance is,

$$
\langle \dot{v}_{sn}^2 \rangle = 2\sigma_s^2 h(\boldsymbol{d_n}), \tag{62}
$$

where $\boldsymbol{d_n} = (d_{1n}, d_{2n}, d_{3n})$. Therefore we can write the upcrossing rate as:

$$
\boxed{\begin{aligned}
r(x_0) = \frac{1}{2\pi}&\sqrt{\frac{\sum_{n=0}^{\infty} h(\boldsymbol{d_n})\phi_n(x_0)^2}{\sum_{n=0}^{\infty} h(\boldsymbol{c_n})\phi_n(x_0)^2}} \\
&\times \exp\left[\frac{-lv_{\text{th}}^2}{4\sigma_s^2\sum_{n=0}^{\infty} h(\boldsymbol{c_n})\phi_n(x_0)^2}\right] .
\end{aligned}} \tag{63}
$$

It is not obvious from (63), but the addition of resonance can either increase or decrease the overall upcrossing rate, depending on the value of v_{th}. For small v_{th}, $r(x_0)$ increases with increasing κ and decreases with increasing α_w; for larger v_{th}, $r(x_0)$ decreases with increasing κ and decreases with increasing α_w. An example of how this changes is shown in FIG. 6. The point of intersection at which the effect of resonance on the firing rate changes from being positive to negative is increased with higher α_w, lower κ and lower α_s.

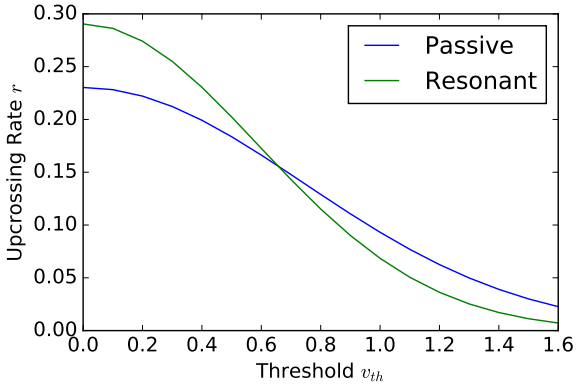

FIG. 6: Comparison of the upcrossing rate between passive and resonant membranes as a function of v_{th} for $x_0 = l/2$, $\alpha_s = 1.1$ and $\sigma_s = 1$. For the resonant membrane $\kappa = 0.85$ and $\alpha_w = 1$.

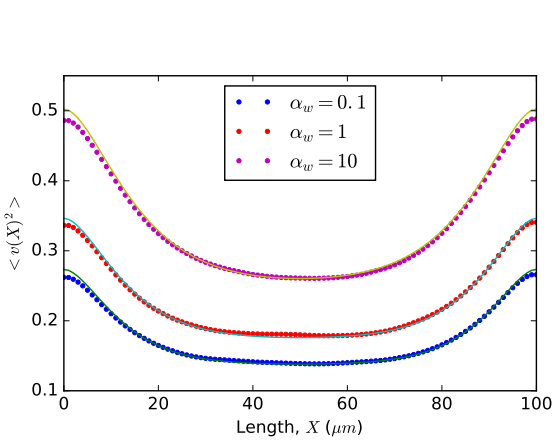

(a) Variance for $\lambda = 20\,\mu\text{m}$, $\alpha_s = 1.1$, $\kappa = 0.85$.

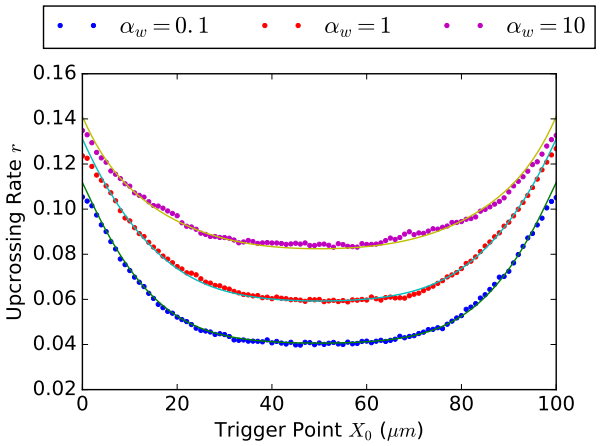

(b) Upcrossing rate for $\lambda = 20\,\mu\text{m}$, $\alpha_s = 1.1$, $\kappa = 0.85$, $v_{\text{th}} = 0.75$.

FIG. 5: Variance and upcrossing rate for a resonant cable subject to filtered noise.

The reason for this intersection is because when v_{th} is small, the exponential term in (63) is ~ 1, meaning the prefactor dominates. Since $\langle \dot{v}(x_0)^2 \rangle / \langle v(x_0)^2 \rangle$ is increased by resonance, this increases $r(x_0)$. On the other hand, as v_{th} becomes larger, the exponential term dominates. As $\langle v(x_0)^2 \rangle$ is decreased by resonance, this will decrease $r(x_0)$.

For simulations of the resonant membrane upcrossing rate, v_{th} was kept at 0.75, while α_w was varied, with the values of 0.1, 1 and 10 again used. For this threshold, it can be seen in FIG. 5b that as α_w is increased, the upcrossing rate increases. Therefore this is an example of resonance lowering the upcrossing rate.

V. CONCLUSION

In all four cases investigated, analytical results for the steady state variance could be derived and understood. For filtered noise, the upcrossing method was successfully employed to approximate the firing rate, expanding the utility of this method to spatially distributed neurons.

Resonance dampened the variance for both white and filtered noise, however its effect on the firing rate was more interesting: increasing it for white noise, while either increasing or decreasing it for filtered noise depending on the threshold. For white noise, further investigation is required to understand this effect.

Future work would include the frequency response of passive and resonant membranes, similar to the approach for point neurons seen in [7]. This would allow spatial analysis of single neuron behaviour to patterned synaptic drive.

Another aspect that could be investigated would be to conduct the simulations with different boundary conditions. Applying zero voltage boundary conditions would be straightforward and has already been done for the passive membrane with white noise in [8]. A particularly useful boundary condition would be to put a lumped soma at one end of the cable. Furthermore, with results for a range of boundary conditions, it becomes possible to model a dendritic tree by matching the boundary conditions at the branch nodes.

[1] A. U. Larkman, the Journal of Comparative Neurology **306**, 332 (1991).
[2] N. Spruston, Nature Reviews Neuroscience **9**, 206 (2008).
[3] R. Yuste and D. W. Tank, **16**, 701 (1996).
[4] A. A. Faisal, L. P. J. Selen, and D. M. Wolpert, Nature Reviews Neuroscience **9**, 292 (2008).
[5] H. Hu, K. Vervaeke, and J. F. Storm, pp. 783–805 (2002).
[6] D. Ulrich, Journal of Neurophysiology **87**, 2753 (2002).
[7] L. Badel, Physical Review E - Statistical, Nonlinear, and Soft Matter Physics **84** (2011).
[8] H. C. Tuckwell and J. B. Walsh, Biological Cybernetics **49**, 99 (1983).
[9] W. Rall, Comprehensive Physiology pp. 39–97 (2011).
[10] I. S. Gradshteyn and I. M. Ryzhik, *Table of integrals, series, and products* (Academic press, 2007).
[11] P. C. Bush and T. J. Sejnowski, Journal of Neuroscience Methods **46**, 159 (1993).
[12] C. Koch, Biological Cybernetics **50**, 15 (1984).
[13] I. Erchova, G. Kreck, U. Heinemann, A. V. M. Herz, and M. Johannes, Journal of Physiology **1**, 89 (2004).
[14] M. J. E. Richardson and W. Gerstner, Neural computation **947**, 923 (2005).
[15] S. O. Rice, The Bell System Technical Journal **24**, 46 (1945).
[16] T. Verechtchaguina, I. M. Sokolov, and L. Schimansky-Geier, BioSystems **89**, 63 (2007).